Observation of the D'yakonov-Perel' Spin Relaxation in Single-Crystalline Pt Thin Films

Jeongchun Ryu, Makoto Kohda, and Junsaku Nitta*
Department of Materials Science, Tohoku University, Sendai 980-8579, Japan
(Received 30 November 2015; revised manuscript received 8 April 2016; published 22 June 2016)

The spin relaxation mechanism in single-crystalline and polycrystalline platinum (Pt) thin films is revealed by a quantum interference effect. Examining the relationship between the spin relaxation rate and momentum scattering rate by changing Pt thickness, we find that the spin relaxation rate of Pt strongly depends on both crystal structure and thickness even though the quality of material (Pt) is unchanged. In particular, the D'yakonov-Perel' mechanism is considered as a dominant mechanism under cases where scattering events are suppressed or the interface effect is not negligible.

DOI: 10.1103/PhysRevLett.116.256802

For the realization of functional spintronic devices, much attention has been focused on spin-orbit interaction (SOI) in both semiconductors and metals [1]. In particular, there have been many practical approaches utilizing the SOI in metals, magnetization reversal of a ferromagnet on top of a heavy paramagnetic metal induced by in-plane current [2,3], or domain wall motion driven by spin-orbit torque [4,5]. These provide an essential technology for the high performance memory devices. Furthermore, for low power logic devices, the spin Seebeck effect [6,7] or spin Hall effect [8–10] in metals with a strong SOI has made remarkable progress in generating pure spin current. These studies indicated that the SOI in paramagnetic heavy metals should be a fundamental ingredient for future spintronic devices. However, it has been reported that the parameters that show the strength of SOI in metals vary greatly with experimental techniques or sample structures, even with the same materials; in the case of Pt, the spin Hall angle has been estimated as $0.012 - 0.37$ and the spin relaxation length varies from 1.5 to 11 nm [3,10–18].

In general, the SOI is described by the following equation:

$$H_{\mathrm{so}} = -\mu_B \sigma \cdot \left(\frac{\vec{p} \times \vec{E}}{2 m_e c^2} \right). \tag{1}$$

Here, μ_B, σ, m_e, and c are the Bohr magnetron, the vector of Pauli matrices, the free electron mass, and the velocity of light, respectively. Thus, it is considered that the electric field $\vec{E}$, where the electrons with the momentum $\vec{p}$ pass through, determines the origin and strength of the SOI. Since the spin relaxation mechanism reflects the origin of the SOI, understanding the spin relaxation mechanism in metals opens up the pathway to explain these confusing results.

There are two mechanisms for spin relaxation induced by the SOI [19]: the Elliot-Yafet (EY) mechanism [20,21] and the D'yakonov-Perel' (DP) mechanism [22–25]. If the metals with the SOI induced by host ions have a center of inversion symmetry, the spin-up and -down states are degenerate, but are admixtures of two spin states. The ordinary scattering by such as phonons and impurities can cause spin relaxation since the momentum $\vec{p}$ and the spin σ are entangled and they no longer make a good quantum number. This is one of the EY spin relaxation mechanisms. If the $\vec{E}$ is induced by nonperiodic components like impurities or crystal grain boundaries, this also results in another EY mechanism. Since the EY mechanism is basically caused by momentum scatterings, more scattering chances make the spin relaxation faster; i.e., the momentum scattering rate Γ_p has a proportional relation to the spin relaxation rate Γ_{so}.

In contrast, it is well known that the DP mechanism appears in III-V compound semiconductors with spatial inversion asymmetry. The lack of spatial inversion breaks spin degeneracy and gives rise to an effective magnetic field, leading to spin precession. In particular, the Rashba SOI [23,24] induced by structural inversion asymmetry is crucial for spintronics since it makes spin manipulation possible by applying an external electric field [26,27]. The DP mechanism is essentially a motion–narrowing effect of spin precession induced by the effective magnetic field. In contrast to the EY mechanism, frequent momentum scattering events suppress spin relaxation. Therefore, Γ_{so} is inversely proportional to Γ_p in the DP mechanism.

Up to now, the EY mechanism based on momentum scattering has been explained as a dominant spin relaxation mechanism in metals because of its short mean-free path. On the other hand, recent studies suggest that the DP mechanism also contributes to spin relaxation in metals. For example, it has been discussed that the Rashba SOI on the interface causes the spin-orbit torque in ferromagnetic metal or paramagnetic metal interfaces [2]. In addition, recent research has proved the existence of the Rashba SOI derived from angle-resolved photoemission (ARPES) and electronic structure calculation on each Ag/Pt (ARPES) and Pt surface (calculation) [28].

There is still a lack of transport data to show the existence of Rashba SOI in metal surfaces or interfaces and how the Rashba SOI quantitatively influences the spin relaxation in metallic systems. If the Rashba SOI is convinced by transport measurements, it should provide great interest in metal-based spintronic fields since the electric field manipulation of spins in metals will be expected [29]. In this study, we have investigated the spin relaxation mechanisms in Pt thin films depending on the Pt thickness and crystal structure by the quantum interference effect, weak antilocalization (WAL), which is a direct method to measure the SOI of materials. In the bulk Pt films, the EY mechanism is regarded as the dominant mechanism. In contrast, if the thickness decreases, the contribution of an interface such as the Rashba SOI cannot be negligible. Likewise, it is considered that a disordered system inducing the scattering promotes the EY mechanism in the case of polycrystalline structure. In other words, we can expect that with single-crystalline Pt, which has periodic lattice structure, the EY mechanism can be suppressed, and then the DP mechanism comes to play an important role for spin relaxation.

Through our research, we find that the spin relaxation rate is clearly dependent on Pt thickness and crystal structure. In the relatively thick films of polycrystalline Pt, the EY mechanism is dominant, as is well known. However, in the thinner films, Γ_{so} deviates from the EY mechanism, so that the DP mechanism turns out to play an indispensable role in explaining those results. Furthermore, in single-crystalline Pt thin films where the scattering events can be suppressed considerably compared to polycrystalline Pt thin films, the spin relaxation is mainly induced by the DP mechanism.

To grow polycrystalline and single-crystalline Pt film, we prepared *i*-GaAs (100) and MgO (111) substrates. The Pt/GaAs and Pt/MgO structures were obtained by radio-frequency sputtering. All samples are covered with an AlO cap layer (0.6 nm) in order to prevent oxidation or any contamination and to induce the Rashba SOI originated by the structure inversion asymmetry on the interface. Figure 1(a) shows each crystallographic structure of Pt/GaAs and Pt/MgO film along the growth direction taken by x-ray diffraction (XRD) measurement. Since the lattice constant of MgO (4.21 Å) is close to that of Pt (3.91 Å); therefore, Pt oriented to the (111) plane can be epitaxially grown on MgO substrate at the high growth temperature (500 °C). On the contrary, the two peaks, not just Pt (111) but also Pt (200), are observed on the GaAs substrate, which indicates polycrystalline structure. The reflection high energy electron diffraction (RHEED) patterns taken after the growth support the finding that the crystallographic quality of Pt/MgO is preserved for both thick (10 nm) and thin (3 nm) Pt films [Figs. 1(b) and 1(c)]. Furthermore, the in-plane XRD (φ-scan) pattern of Pt/MgO in Fig. 1(d) shows sixfold symmetry for Pt (111),

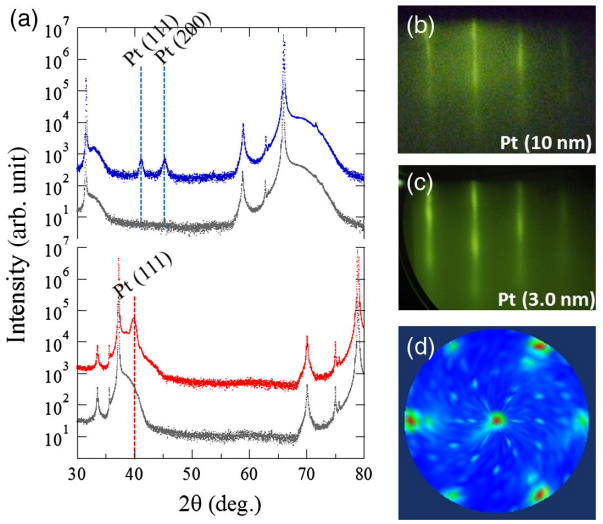

FIG. 1. (a) XRD results for Pt/GaAs (blue dots) and Pt/MgO (red dots). For comparing to the substrate, the corresponding XRD peaks of each substrate are described under the Pt peaks. (b),(c) RHEED patterns for single-crystalline Pt on MgO substrate with 10 nm thickness and 3.0 nm thickness, respectively. (d) Results of φ scan of Pt/MgO film. The three peaks of Pt overlapping those of the MgO substrate show stronger signals than the other three peaks of Pt.

clearly indicating that the single-crystalline Pt is successfully grown on MgO (111) with a lattice matched relationship [30–32]. To measure the thickness dependence, the Pt films on both substrates have different thickness d: from 2 to 15 nm. To obtain transport parameters, we fabricated the simple Hall bar structure on both Pt crystal structures with $20\ \mu\text{m}\ (\text{width}) \times 160\ \mu\text{m}\ (\text{length})$ by using photolithography. The result of sheet resistance for both films in Fig. 2(a) plainly shows the dependence of crystal structure and Pt thickness. The Γ_p can be derived by the equation $\Gamma_p = E_F/Dm^*$, where E_F, D, and m^* indicate, respectively, Fermi energy, diffusion constant, and the effective mass. Consequently, we can obtain the relationship between Γ_p to Pt thickness in two different crystal structures [Fig. 2(b)]. The Pt thickness dependence of D is also shown in Fig. 2(c) for understanding the change of Γ_p. The transport properties shown in Fig. 2 indicate that Γ_p of polycrystalline is even larger than that of single-crystalline film in the entire Pt thickness region, which suggests that scattering events are more suppressed in single-crystalline Pt film. The momentum scattering increases drastically with decreasing thickness; therefore, the scattering on the interfaces has a great influence in the case of thin Pt film. Then the interface scattering probability C_{inf} is quantitatively introduced. C_{inf} means the ratio of conduction electrons going through the interface with respect to entire conduction electrons. Accordingly, C_{inf} is calculated as followings: $C_{\text{inf}} = \Gamma_{p,\text{interface}}/\Gamma_p$, where $\Gamma_p = \Gamma_{p,\text{interface}} + \Gamma_{p,\text{bulk}}$. We posit that $\Gamma_{p,\text{bulk}}$ is the same as Γ_p of the Pt film with 15 nm thickness because

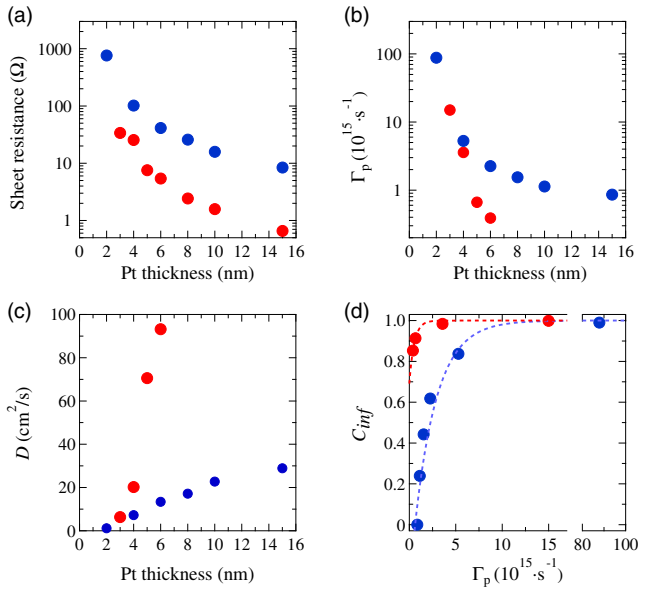

FIG. 2. Marks for polycrystalline Pt/GaAs and for single-crystalline Pt/MgO correspond to blue dots and red dots, respectively. (a) Sheet resistance depending on thickness. (b) Γ_p as a function of Pt thickness. It shows that Γ_p increases with decreasing Pt thickness. The scale of the y axis is logarithmically plotted. (c) Diffusion constant with respect to Pt thickness is shown for easy understanding of Γ_p. (d) Γ_p dependence of interface scattering probability.

of enough low sheet resistance to neglect the influence of interface scattering. Then we obtain the relationship in Fig. 2(d) that C_{inf} drastically increases with decreasing Pt thickness in both crystal structures.

In order to evaluate Γ_{so}, the WAL analysis [37–39] was performed from magnetoconductance measured by the four-terminal technique at $T = 1.6$ K. Pt thickness dependences of normalized magnetoresistance for both polycrystalline Pt and single-crystalline Pt films are shown in Figs. 3(a) and 3(b). In the case of single-crystalline Pt films, because of the high mobility, the classical magnetoresistance is observed predominantly in the thick Pt region [40,41]. Such a classical magnetoresistance should be subtracted to obtain the pure quantum interference effect. In this experiment, we obtained it by subtracting the parabolic dependence approximated in the low magnetic field from the raw magnetoresistance. One instance of this approach is introduced in Fig. 3(e). For samples with thickness over 6 nm, however, we could not extract the proper quantum interference effect due to its too high mobility and low resistivity. Accordingly, the quantum interference effect in single-crystalline films is able to be obtained only under 6 nm Pt thickness. Concentrating on the quantum interference effect, since Pt is known as a strong SOI material, all samples show WAL. However, as shown in Figs. 3(c) and 3(d), the amplitude of WAL for each Pt film is entirely different, depending on thickness and crystal structure. For example, even in the same crystal

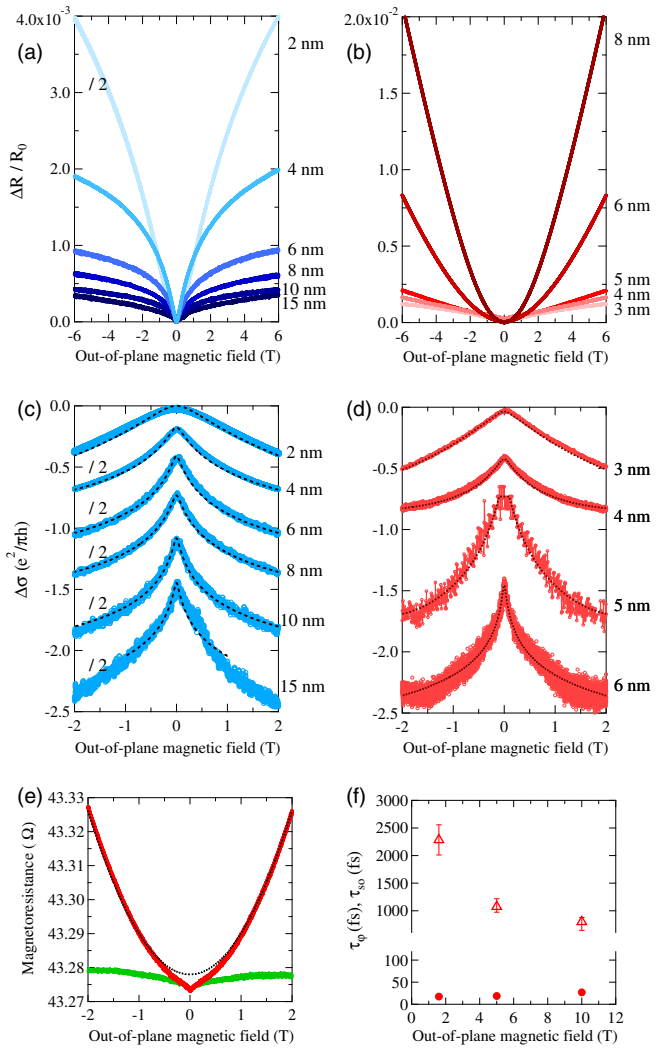

FIG. 3. Normalized magnetoresistance results for (a) polycrystalline Pt/GaAs and (b) single-crystalline Pt/MgO depending on different Pt thickness. The gradation from dark color to light color of each result corresponds to change of Pt thickness from thick film to thin film. WAL curves for (c) polycrystalline Pt/GaAs (blue lines) and (d) single-crystalline Pt/MgO (red lines). Dark dotted lines are best fitted results based on HLN and ILP theories. (e) Example of subtracting the classical magnetoresistance in single-crystalline Pt film with 4.0 nm thickness. Red dots and black line indicate the raw data we obtained and the resistance induced by the classical magnetoresistance, respectively. By subtracting the black line from the red dots, we can extract the innate magnetoresistance originated by the SOI (green dots). (f) τ_φ (triangle) and τ_{so} (circle) in single-crystalline Pt film with 5.0 nm thickness depending on the temperature.

structure, the amplitude of magnetoconductance $\Delta\sigma[= \sigma(B) - \sigma(0)]$ gradually decreases as the Pt thickness also decreases. Additionally, even though the Pt thickness is equal, the amplitude of $\Delta\sigma$ depends on its crystal structure. As we confirmed from the temperature dependence of τ_φ and τ_{so} [Fig. 3(f)], the obtained quantum interference effect after subtracting classical magnetoresistance is appropriate:

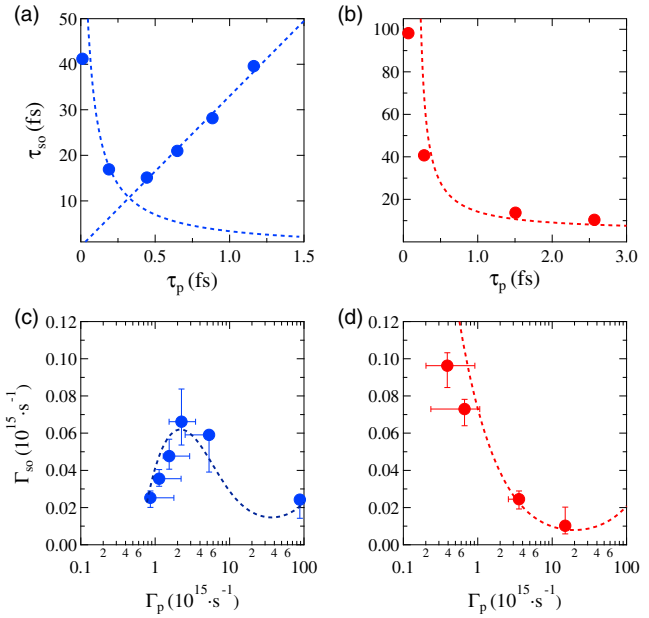

FIG. 4. The relationship between τ_p and τ_{so} for (a) polycrystalline Pt films (b) single-crystalline Pt films. The guide lines of the EY mechanism ($\tau_{so} \propto \tau_p$) and DP mechanism ($\tau_{so} \propto {\tau_p}^{-1}$) are introduced as the dotted lines to help qualitative understanding. (c),(d) Relationship between Γ_{so} and Γ_p for polycrystalline Pt films and single-crystalline Pt films, respectively. The x axis of (c) and (d) is described in logarithmic scale. The blue dotted line in (c) and the red dotted line in (d) indicate the best fit of spin relaxation mechanism based on Eq. (2). In (c), the fitted line starts on Γ_p of the Pt film with 15 nm thickness since we defined C_{inf} as zero in the Pt film with 15 nm thickness.

the phase coherence time τ_φ, determining the limit of WAL, highly decreases with decreasing temperature although $\Gamma_{so}(=\tau_{so}^{-1})$ is nearly constant [42–44].

Clarifying the above results, we focused on the spin relaxation mechanism. First of all, to estimate the spin relaxation rate Γ_{so} quantitatively, we fitted the obtained data to theoretical formulas. The results can be analyzed by two theories of quantum correction of the conductance: the Hikami-Larkin-Nagaoka (HLN) formula for polycrystalline Pt films and the Iordanskii–Lyanda-Geller–Pikus (ILP) formula for single-crystalline Pt films [33,34]. Even though the obtained results are well matched to both theories, we should consider that the magnetoconductance for polycrystalline Pt films should be fitted to the HLN theory because the HLN theory takes into account the EY mechanism. On the other hand, the ILP theory is suitable for single-crystalline Pt films where the scattering events are highly suppressed.

To begin with the spin relaxation mechanism in polycrystalline Pt films [Fig. 4(a)], the linear relationship represents that the EY mechanism exists in the thick Pt region as already known in metals. However, deviation from the linear dependence of the EY mechanism is observed in the thin Pt region, especially under 4 nm thickness. Indeed, τ_{so} in this region is significantly enhanced; therefore, this suggests that the existence of the DP mechanism is required. Secondly, focusing on the spin relaxation mechanism in single-crystalline Pt films [Fig. 4(b)], Γ_{so} is definitely apart from the relationship of the EY mechanism in the entire region. It is likely that τ_{so} is inversely proportional to τ_p rather than having a linear relationship, indicating the DP mechanism.

The tendencies plotted in Figs. 4(a) and 4(b) are absolutely exotic: even though Γ_p drastically increases with decreasing Pt thickness in both crystal structures, Γ_{so} shows itself to be significantly suppressed rather than enhanced. Consequently, it is essential to put both the DP and EY mechanisms together. Considering that the conduction electrons are greatly influenced by the interface, as we discussed in transport measurement [Fig. 2(d)], the contributions related to the interface should be taken into account in both the EY mechanism and the DP mechanism: the EY mechanism on the interface and the Rashba SOI induced by the potential gradient on the interface. Hence, the Γ_{so} taking into account both the EY mechanism and the DP mechanism is expressed as

$$\Gamma_{so} = (1 - C_{\mathrm{inf}})\varepsilon_b \Gamma_p + C_{\mathrm{inf}}\varepsilon_i \Gamma_p + C_{\mathrm{inf}}\left(\frac{\Delta_R}{\hbar}\right)^2 \Gamma_p^{-1}. \quad (2)$$

Here, ε_b, ε_i, and Δ_R mean the spin-flip probability in the bulk Pt system, the spin-flip probability on the interface, and the spin-splitting energy created by the interface Rashba SOI. For the EY mechanism at the interface and the interface Rashba SOI, C_{inf} is put in as a coefficient because the higher probability passing through the interface indicates that the EY mechanism on the interface and the Rashba SOI are enhanced on its spin relaxation mechanism; and vice versa, $(1 - C_{\mathrm{inf}})$ is inserted for the EY mechanism for the bulk system.

Applying Eq. (2) on Γ_{so} with both crystal structures, we find that the behaviors, which neither the EY mechanism nor the DP mechanism alone can cover, have been completely explained as shown in Figs. 4(c) and 4(d). Looking over the fitted parameters in detail, first of all, $\varepsilon_{b,\mathrm{poly}}$ is estimated as 1.99×10^{-3}, whereas $\varepsilon_{b,\mathrm{epi}}$ is less than 0.50×10^{-3}, at least 4 times smaller than $\varepsilon_{b,\mathrm{poly}}$. A comparison between $\varepsilon_{b,\mathrm{poly}}$ and $\varepsilon_{b,\mathrm{epi}}$ evidently corresponds to the assumption that single-crystalline films suppressed the EY mechanism. Note that we made the ε_i consistent for both crystal structures in this analysis as 0.20×10^{-3}, which has the same order with the probability known before [17,45]. The factor Δ_R shows a difference as well, depending on the crystal structure: $\Delta_{R,\mathrm{poly}} = 3.42 \times 10^{-1}$ (eV) and $\Delta_{R,\mathrm{epi}} = 1.85 \times 10^{-1}$ (eV), which reflects that the interface, not only between Pt and AlO cap layer but also between Pt and the substrate, makes the main contribution to the Rashba SOI. Since the Rashba SOI is expected to be tunable by an electric field [29], we observed

the change of WAL by applying external gate voltage on a 3 nm thickness single-crystalline Pt film [32]. It evidently supports that the Rashba SOI plays a great role in spin relaxation.

In conclusion, we experimentally clarify the spin relaxation mechanism in Pt films from the relationship between Γ_{so} and Γ_p and find out that spin relaxation depends on the crystal structure and thickness of Pt films although the material Pt is never changed. These exotic phenomena can be explained by combining not just the EY mechanism but also the DP mechanism, originating from the Rashba SOI. Hence, all our results verify that the spin relaxation in metals is determined by contributions of the DP mechanism in addition to the EY mechanism, whereas the dominant contribution is determined by the characteristics of the system. This achievement proposes the possibility of gate-controlled SOI as well as a fundamental understanding of spin relaxation in metals, which are indispensable components for designing future spintronic devices.

This work was supported by the Japan Society for the Promotion of Science with Grant-in-Aid No. 15H05699, No. 25220604, No. 15H02099, and No. 15H05854. The authors thank Professor N. Tezuka, Professor J. Shiogai, and Dr. T. Miyazaki for discussions on Pt growth and evaluation of crystal structure. Technical support from R. Ohsugi, F. Nagasawa, S. Takasuna, K. Yoshizumi, M. Kong, and H. Gamou is acknowledged. J. R. acknowledges financial support from "ITO Foundations for International Education and Exchange."

*nitta@material.tohoku.ac.jp

[1] A. Manchon, H. C. Koo, J. Nitta, S. M. Frolov, and R. A. Duine, Nat. Mater. **14**, 871 (2015).
[2] I. M. Miron *et al.*, Nat. Mater. **9**, 230 (2010); I. M. Miron, K. Garello, G. Gaudin, P.-J. Zermatten, M. V. Costache, S. Auffret, S. Bandiera, B. Rodmacq, A. Schuhl, and P. Gambardella, Nature (London) **476**, 189 (2011).
[3] L. Liu, O. J. Lee, T. J. Gudmundsen, D. C. Ralph, and R. A. Buhrman, Phys. Rev. Lett. **109**, 096602 (2012).
[4] M. Yamanouchi, D. Chiba, F. Matsukura, and H. Ohno, Nature (London) **428**, 539 (2004).
[5] T. Koyama *et al.*, Nat. Mater. **10**, 194 (2011).
[6] K. Uchida, S. Takahashi, K. Harii, J. Ieda, W. Koshibae, K. Ando, S. Maekawa, and E. Saitoh, Nature (London) **455**, 778 (2008).
[7] K. Uchida, M. Ishida, T. Kikkawa, A. Kirihara, T. Murakami, and E. Saitoh, J. Phys. Condens. Matter **26**, 343202 (2014).
[8] Y. K. Kato, R. C. Myers, A. C. Gossard, and D. D. Awschalom, Science **306**, 1910 (2004).
[9] S. Takahashi and S. Maekawa, Phys. Rev. Lett. **88**, 116601 (2002).
[10] T. Kimura, Y. Otani, T. Sato, S. Takahashi, and S. Maekawa, Phys. Rev. Lett. **98**, 156601 (2007).
[11] M. Morota, Y. Niimi, K. Ohnishi, D. H. Wei, T. Tanaka, H. Kontani, T. Kimura, and Y. Otani, Phys. Rev. B **83**, 174405 (2011).
[12] K. Ando *et al.*, J. Appl. Phys. **109**, 103913 (2011).
[13] M. Weiler *et al.*, Phys. Rev. Lett. **111**, 176601 (2013).
[14] V. Castel, N. Vlietstra, J. B. Youssef, and B. J. V. Wees, Appl. Phys. Lett. **101**, 132414 (2012).
[15] Z. Qiu, K. Ando, K. Uchida, Y. Kajiwara, R. Takahashi, H. Nakayama, T. An, Y. Fujikawa, and E. Saitoh, Appl. Phys. Lett. **103**, 092404 (2013).
[16] M. Althammer *et al.*, Phys. Rev. B **87**, 224401 (2013).
[17] H. Nakayama, K. Ando, K. Harii, T. Yoshino, R. Takahashi, Y. Kajiwara, K. Uchida, Y. Fujikawa, and E. Saitoh, Phys. Rev. B **85**, 144408 (2012).
[18] Y. Niimi, D. Wei, H. Idzuchi, T. Wakamura, T. Kato, and Y. Otani, Phys. Rev. Lett. **110**, 016805 (2013).
[19] J. Fabian, A. Matos-Abiague, C. Ertler, P. Stano, and I. Žutić, Acta Phys. Slovaca **57**, 565 (2007).
[20] R. J. Elliott, Phys. Rev. **96**, 266 (1954).
[21] Y. Yafet, Phys. Rev. **85**, 478 (1952).
[22] M. I. D'yakonov and V. I. Perel', Zh. Eksp. Teor. Fiz. **60**, 1954 (1971) [Sov. Phys. JETP **33**, 1053 (1971)].
[23] E. I. Rashba, Fiz. Tverd. Tela (Leningrad) **2**, 1224 (1960) [Sov. Phys. Solid State **2**, 1109 (1960)].
[24] E. I. Rashba and Yu A. Bychkov, J. Phys. C **17**, 6039 (1984).
[25] G. Dresselhaus, Phys. Rev. **100**, 540 (1955).
[26] J. Nitta, T. Akazaki, H. Takayanagi, and T. Enoki, Phys. Rev. Lett. **78**, 1335 (1997).
[27] T. Bergsten, T. Kobayashi, Y. Sekine, and J. Nitta, Phys. Rev. Lett. **97**, 196803 (2006).
[28] A. Bendounan, K. Aït-Mansour, J. Braun, J. Minár, S. Bornemann, R. Fasel, O. Gröning, F. Sirotti, and H. Ebert, Phys. Rev. B **83**, 195427 (2011).
[29] S.-J. Gong, C.-G. Duan, Y. Zhu, Z.-Q. Zhu, and J.-H. Chu, Phys. Rev. B **87**, 035403 (2013).
[30] http://crystdb.nims.go.jp/crystdb/.
[31] B. M. Lairson, M. R. Visokay, R. Sinclair, S. Hagstrom, and B. M. Clemens, Appl. Phys. Lett. **61**, 1390 (1992).
[32] See Supplemental Material at http://link.aps.org/supplemental/10.1103/PhysRevLett.116.256802, which includes Refs. [33–36], for details about Pt growth and gate voltage dependence of magneto conductance.
[33] S. Hikami, A. I. Larkin, and Y. Nagaoka, Prog. Theor. Phys. **63**, 707 (1980).
[34] S. V. Iordanskii, Yu. B. Lyanda-Geller, and G. E. Pikus, JETP Lett. **60**, 206 (1994); C. Schierholz, T. Matsuyama, U. Merkt, and G. Meier, Phys. Rev. B **70**, 233311 (2004).
[35] H. Nakayama, J. Ye, T. Ohtani, Y. Fujikawa, K. Ando, Y. Iwasa, and E. Saitoh, Appl. Phys. Express **5**, 023002 (2012).
[36] S. Shimizu, K. S. Takahashi, T. Hatano, M. Kawasaki, Y. Tokura, and Y. Iwasa, Phys. Rev. Lett. **111**, 216803 (2013).
[37] G. Bergmann, Phys. Rev. Lett. **48**, 1046 (1982).
[38] G. Bergmann, Phys. Rev. B **28**, 2914 (1983).
[39] M. Kohda, T. Bergsten, and J. Nitta, J. Phys. Soc. Jpn. **77**, 031008 (2008).
[40] A. A. Abrikosov, *Fundamentals of the Theory of Metals* (North-Holland, Amsterdam, 1988).

[41] K. Liu, C. L. Chien, P. C. Searson, and K. Yu-Zhang, Appl. Phys. Lett. **73**, 1436 (1998).
[42] D. A. Poole, M. Pepper, and A. Hughes, J. Phys. C **15**, L1137 (1982).
[43] S. A. Studenikin, P. T. Coleridge, N. Ahmed, P. J. Poole, and A. Sachrajda, Phys. Rev. B **68**, 035317 (2003).
[44] A. E. Hansen, M. T. Björk, C. Fasth, C. Thelander, and L. Samuelson, Phys. Rev. B **71**, 205328 (2005).
[45] F. J. Jedema, A. T. Filip, and B. J. van Wees, Nature (London) **410**, 345 (2001); F. J. Jedema, M. S. Nijboer, A. T. Filip, and B. J. van Wees, Phys. Rev. B **67**, 085319 (2003).